Raman and Infrared Structural Investigation of (PbO)x(ZnO)(0.6-x)(P2O5)0.4 glasses

G. Le Saout, P. Simon, F. Fayon, Annie Blin, Yann Vaills

Raman and Infrared Structural Investigation of $(PbO)_x(ZnO)_{(0.6-x)}(P_2O_5)_{0.4}$ glasses

Gwenn Le Saoût,[1,2,#] Patrick Simon,[1,2,*] Franck Fayon,[1,2] Annie Blin,[1,2] Yann Vaills[1,2]

1 - CNRS, UPR3079 CEMHTI, 45071 Orléans Cedex 2, France

2 - Université d'Orléans, BP 6749, 45067 Orléans Cedex 2, France

*Corresponding author.

E-mail address: simon@cnrs-orleans.fr

[#] Present address :Laboratory of Construction Materials, EPFL, CH – 1015 Lausanne

Abstract

The structure of ternary $(PbO)_x(ZnO)_{(0.6-x)}(P_2O_5)_{0.4}$ glasses was investigated using Raman scattering and infrared spectroscopy over the compositional range x = 0 to 0.6. No significant change of the average chain length composed by PO_4 tetrahedral units with the substitution of zinc for lead cation was observed. The linewidth and frequency variations of the Raman high-frequency bands reflect the Zn/Pb substitution in these glasses and are correlated with the metal oxygen force constant and local disorder. The infrared reflectivity spectra have been fitted with the four-parameter dielectric function model. The variation in the 1000-1200 cm^{-1} frequency range has been attributed to an increase of the oscillator damping Γ_{LO} $(PO_3)^{2-}{}_{as}$ with PbO content vibrations rather than a variation of the chain length.

KEYWORDS: phosphate glasses; Raman; infrared reflectivity;

1. Introduction

Compared with conventional oxide glasses, phosphate glasses have low melting temperature, high thermal expansion coefficients and high electric conductivity. These properties make them candidates for a variety of technological applications, from rare-earth ion hosts for solid state lasers to low-temperature sealing glasses.[1] The addition of one or more oxides such as PbO, ZnO, Al_2O_3 or Fe_2O_3 leads to an improvement in the chemical durability of the modified phosphate glasses.[2] The properties that make modified phosphate glasses candidates for many different applications are related to their molecular-level structures.

Vitreous P_2O_5 (v-P_2O_5) has its structure based on corner–linked PO_4 tetrahedra, each tetrahedron having three bridging oxygens and one doubly bonded oxygen thereby satisfying the +5 valence of phosphorus.[3] The addition of modifier cation M to v-P_2O_5 results in the creation of non-bridging oxygens O^{NB} at the expense of bridging oxygens O^B. Thus, in $(MO)_x(P_2O_5)_{(1-x)}$ glasses, the depolymerisation of the phosphate network above the metaphosphate region ($x \geq 0.5$) can be described by these disproportionation reactions :[4]

$$2\left[-O^B-\left(PO_2^{NB}\right)^--O^B-\right]\overset{k_2}{\Leftrightarrow}\left[O^{NB}=PO_3^B\right]+\left[-O^B-\left(PO_3^{NB}\right)^{2-}\right] \quad (1)$$

$$2\left[-O^B-\left(PO_3^{NB}\right)^{2-}\right]\overset{k_1}{\Leftrightarrow}\left[-O^B-\left(PO_2^{NB}\right)^--O^B-\right]+\left[\left(PO_4^{NB}\right)^{3-}\right] \quad (2)$$

In the $(PbO)_x(ZnO)_{(0.6-x)}(P_2O_5)_{0.4}$ glasses, previous ^{31}P NMR quantitative measurements[5] reveal no significant change of the phosphate group distributions (number of $\left[-O^B-\left(PO_3^{NB}\right)^{2-}\right]$ = number of $\left[-O^B-\left(PO_2^{NB}\right)^--O^B-\right]$) with the substitution of zinc for lead cation. This behaviour reflects low disproportionation reaction constants similar to those measured for binary $(ZnO)_x(P_2O_5)_{(1-x)}$[6] and

$(PbO)_x(P_2O_5)_{(1-x)}$[7] phosphate glasses. We present here the analysis and discussion of Raman and infrared spectra for the same samples, following the preliminary results given in ref. 5. Attention is focused on the high-frequency part of the spectra (600-1500 cm^{-1}), corresponding to the characteristic features of the phosphate network.

2. Experiment and data reduction

The $(PbO)_x(ZnO)_{(0.6-x)}(P_2O_5)_{0.4}$ samples were prepared from stoichiometric powders resulting from the mixing of $(NH_4)_2HPO_4$, $Pb(NO_3)_2$ and $Zn(NO_3)_2$ aqueous solutions (x=0, 0.1, 0.2, 0.3, 0.4, 0.5 and 0.6). The mixtures were melted in Pt crucibles for one hour at a temperature varying from 800 to 1000°C depending on composition and the melt was poured onto a stainless slab. All sample compositions were checked by chemical analysis (1 mol.% uncertainties). The glass samples ($10\times10\times10$ mm^3) were polished using ethanol and opaline at the final stage.

The Raman spectra have been recorded on a T 64000 Jobin Yvon spectrometer using the λ_0=514.5 nm wavelength of a Coherent Innova 70 Spectrum Argon-Krypton laser. Detection was made with a cooled CCD multichannel detector. Measurements were done in macro-Raman configuration in a right-angle scattering geometry; the laser power focused on the sample is about 0.4 W at the laser output. In order to eliminate the temperature and ω^4 scattering dependences, we always present the reduced intensity, I_{RED}, obtained from the equation:

$$I_{RED}(\omega) = I(\omega)\frac{1}{[1+n(\omega)](\omega_0-\omega)^4} \qquad (3)$$

where $I(\omega)$ is the experimental Raman intensity and $n(\omega)$ is the Bose-Einstein population factor. Care was taken of other processes than 1st order Raman scattering (2nd order Raman, luminescence) through checking of this correction on a typical

sample with four excitation wavelengths (1064 – 647- 514 – 488 nm) : both resulting Raman susceptibilities are identical.

Infrared spectra are performed through measurements of reflection spectra that give access to longitudinal and transverse modes components of each vibrational polar mode while absorption spectroscopy mainly probes transverse modes.[8] Infrared reflectivity spectra were recorded near normal incidence using a Fourier Transform scanning interferometer (Bruker IFS 113v), covering the wave number range 10-12000 cm^{-1} with an effective spectral resolution of 6 cm^{-1}. The dielectric function was deduced by use of two methods: the Kramers-Kronig analysis and a dispersion analysis involving the four-parameter dielectric function model:[9]

$$\varepsilon(\omega)=\varepsilon_\infty\prod_{j=1}^{J}\frac{\omega_{jLO}^2-\omega^2+i\omega\Gamma_{jLO}}{\omega_{jTO}^2-\omega^2+i\omega\Gamma_{jTO}} \qquad (4)$$

where ε_∞ is the high-frequency limit of ε, ω_{jLO}, ω_{jTO} are the longitudinal and transverse oscillator frequencies and Γ_{jLO}, Γ_{jTO} denote longitudinal and transverse damping respectively. For each polar mode, the dielectric strength $\Delta\varepsilon_j$ (strength of the TO component) was calculated from the set of TO-LO splittings:

$$\Delta\varepsilon_j=\frac{\varepsilon_\infty}{\omega_{jTO}^2}\frac{\prod_k\left(\omega_{kLO}^2-\omega_{jTO}^2\right)}{\prod_{k\neq j}\left(\omega_{kLO}^2-\omega_{jTO}^2\right)} \qquad (5)$$

The Kramers-Kronig transform has the advantage over the dispersion analysis to involve no microscopic physical model and is not connected to any particular band shape. On the other hand, the dispersion analysis does not require extrapolation of experimental reflectivity data between 0 and $+\infty$ that are crucial for the Kramers-Kronig transform. Thus, these two methods should be considered to complement each other (see, for discussion and examples, Efimov[10] and references therein) and were

systematically applied to the reflection spectra of $(PbO)_x(ZnO)_{(0.6-x)}(P_2O_5)_{0.4}$ glasses and provided practically coinciding optical constants. Then more sophisticated methods (such as developed in ref. 11) do not need to used here.

3. Results and discussion

The general patterns of the IR reflection spectra of $(PbO)_x(ZnO)_{(0.6-x)}(P_2O_5)_{0.4}$ in the range 10-1500 cm^{-1} are shown in figure 1. The 1500-5500 cm^{-1} range that was also recorded shows no feature at all. Twelve oscillators were used to fit the most pronounced spectral features and the corresponding parameters for the five oscillators used in the high frequency region are listed in table 1 for three compositions (x=0, 0.3 and 0.6). The imaginary parts of the dielectric function (TO-mode structure) and the imaginary parts of the inverse dielectric function (LO-mode structure) in the range 600-1500 cm^{-1} are shown in Fig.2.a. Fig.2.b. displays the Raman spectra in the VV polarisation. The Raman and IR bands assignments of binary $(PbO)_x(P_2O_5)_{(1-x)}$ have been given in a previous paper[12] and are recalled in Table 2 for $(PbO)_{0.6}(P_2O_5)_{0.4}$ glasses.

From the peak positions of $(PO_2)^-$ and (POP) bands, one can note that there is a general softening of the modes in the ternary $(PbO)_x(ZnO)_{(0.6-x)}(P_2O_5)_{0.4}$ glasses upon increasing PbO content (Fig.3). For mixed alkali metaphosphate glasses, Rouse *et al.*[13] have designed a simple vibrational model for the $(PO_2)^-$ unit which indicates that the observed frequency decrease in the $(PO_2)^-$ vibrational bands may be a natural consequence of the decrease in the metal oxygen force constant, resulting from substitution of a smaller cation for a larger one. These behaviours are consistent with previous studies of phosphate glasses[14, 15, 16] indicating that a decrease of the counterion field strength leads to a decrease in these frequencies. Thus, the shift of the $(PO_2)^-$ bands

to lower frequencies may be explained by a decrease of the metal oxygen force constant and evidences a less rigid structure with PbO addition. Indeed, we have observed in a previous study[17] a decrease of the elastic constant C_{11} and of the glass transition temperature with PbO addition that are correlate with the decrease of the ability of the cation to cross-link between different phosphate chains.

For the Raman response, a complete description of absolute Raman scattering intensity from vibration optic modes in glasses is lacking and would require a detailed knowledge of structure and chemistry of bonding (see Lines *et al.*[18, 19]). However, in the wavenumber range 850-1500 cm^{-1} that corresponds to stretching vibrations in phosphate glasses and if no important coupling between vibrations occurs, all relative Raman intensities can be directly compared.[12] Absolute intensities of these bands are strongly influenced by the kind of metal modifier as previously noticed in metaphosphate glasses.[20] The narrowing of the Raman high frequency bands with PbO addition indicate a weaker distribution of P-O bond lengths and of P-O-P and O-P-O angles in agreement with previous ^{31}P NMR results that show a decrease of ^{31}P NMR linewidth.[5] This shows that the interaction between the phosphate network and Zn^{2+} cations is important, as expected from variation of the Raman high frequency modes. The broadening of the Raman bands with increasing ZnO content leads to band overlapping and do not permit an unambiguous curve-fitting. However, it looks that there is no appearance of extra bands and that the relative intensities of the different components in the 850-1500 cm^{-1} frequency range do not reveal any significant variation upon increasing PbO content. This means that there is no quantitative major variation of the $(PO_2)^-$ and $(PO_3)^{2-}$ groups with the lead content in agreement with previous ^{31}P NMR results that show low

disproportionation reaction constants similar for binary $ZnO-P_2O_5$[6], $PbO-P_2O_5$[7] and ternary $(PbO)_x(ZnO)_{(0.6-x)}(P_2O_5)_{0.4}$[5] glasses.

For the P-O-P band, the effect of cation substitution is less important in the frequency and absolute intensity variations in the Raman spectra because the metal cation interacts weakly with the bridging oxygens.[14] This results in a strongly variation of the relative intensities of the P-O-P band and $(PO_2)^-$ band with the substitution of zinc for lead cation as previously observed in different binary metaphosphate glasses. [14, 20, 21]

We can easily follow the ν_{as}(P-O-P) and $\nu_{as}(PO_2)^-$ vibrations in the IR spectra, located at (889-909 cm^{-1}) and (1196-1251 cm^{-1}) for $(PbO)_{0.6}(P_2O_5)_{0.4}$, with the substitution of lead for zinc cation. The intensity of these bands shown in Figure 4.b. reveals no appreciable systematic changes with glass composition in agreement with previous ^{31}P NMR results. Also based on data presented in Table 1, the bands in the frequency range 1000-1200 cm^{-1} can be related to the $\nu_{as}(PO_3)^{2-}$ vibration and show in Figure 4.b. an opposite variation of the transverse oscillator strength with glass composition. However, Raman and ^{31}P NMR results[5] show us no significant variation of the structural units $(PO_2)^-$ and $(PO_3)^{2-}$ present in the phosphate network. Thus, the variations are due mostly to the intensity redistribution between the two components of the $\nu_{as}(PO_3)^{2-}$ rather than to changes in the relative concentrations of different structural groups. This effect has also been observed by Efimov in pyrophosphate glasses $(Na_2O)_x(ZnO)_{(0.33-x)}(P_2O_5)_{0.66}$ glasses with the substitution of sodium for zinc cation[22] by simulating infrared spectra with a dispersion analysis specific for glasses. According to Efimov, the occurrence of two $(PO_3)^{2-}$ bands indicates a two-site effect and the intensity changes with the substitution of sodium for zinc cation may indicate variations in the symmetry of the phonon localization regions associated with changes in bond and

torsion angles.[23] The curve fitting shows that the reflectivity variation in the 1000-1200 cm^{-1} frequency range appears to be mainly due to the increase of the oscillator damping $\Gamma_{10,LO}$ whereas other linewidths decrease with PbO content (Fig. 4.a). The increase of the oscillator damping may be related to a higher anisotropy along the chain axis compared to the vibration perpendicular to the axe of the ν_3 mode of the end chain tetrahedron. Nevertheless, the interpretation and modelling of IR reflectance spectra of glasses are still difficult and need further improvements [24].

4. Conclusion

Using Raman and infrared spectroscopies, we have investigated the structure of ternary $(PbO)_x(ZnO)_{(0.6-x)}(P_2O_5)_{0.4}$ glasses over the compositional range from x = 0 to 0.6. The linewidths and frequencies variations of the Raman high-frequency bands reflect the Zn/Pb substitution in these glasses and are correlated with the metal oxygen force constant and local disorder. The infrared reflectivity variation in the 1000-1200 cm^{-1} frequency range has been attributed to an increase of the $(PO_3)^{2-}$ oscillator LO damping with PbO content. The intensity variation in the high frequency part of the Raman and IR spectra are attributed to an effect of the Zn/Pb substitution on the vibrational mode of the phosphate chain rather than a variation of the chain length with PbO content.

References

[1] Brow RK. *J. Non-Cryst. Solids* 2000; **263-264**: 1.

[2] Liu HS, Shih PY, Chin TS. *Phys. Chem. Glasses* 1998; **37**: 227.

[3] Suzuya K, Price DL, Loong CK, Martin SW. *J. Non-Cryst. Solids* 1998; **232-234**: 650.

[4] Van Wazer JR. *Phosphorus and Its Compounds*, vol.1. Interscience, New- York, 1958.

[5] Le Saoût G, Fayon F, Bessada C, Simon P, Blin A, Vaills Y. *J. Non-Cryst. Solids* 2001 ; **293-295** : 657.

[6] Brow RK, Tallant DR, Myers ST, Phifer CC. *J. Non-Cryst. Solids* 1995 ; **191** : 45.

[7] Fayon F, Bessada C, Coutures JP, Massiot D. *Inorg. Chem*. 1999; **38**: 5212.

[8] Kamitsos EI, Yiannopoulos YD, Varsamis CP, Jain H. *J. Non-Cryst. Solids* 1997 ; **222**: 59.

[9] Gervais F. In *Infrared and Millimeter Waves*, vol 8, Button KJ (ed.). Academic Press: New York, 1983: 279.

[10] Efimov E. *J. Non-Cryst. Solids* 1999 ; **253** : 95.

[11] De Sousa Meneses D., Rousseau B., Echegut P., Simon P. *Applied Spectroscopy* 2007, **61**, 1390 ; and De Sousa Meneses D., Brun J.F., Echegut P., Simon P. *Applied Spectroscopy* 2004, **58**, 969.

[12] Le Saoût G, Simon P, Fayon F, Blin A, Vaills Y. *J. Raman Spect.* 2002 ; **33**: 740.

[13] Rouse GB, Miller PJ, Risen WM. *J. Non-Cryst. Solids* 1978 ; **28** : 193.

[14] Nelson BN, Exharhos GJ. *J. Chem. Phys*. 1979; **71**: 2739.

[15] Hudgens JJ, Brow RK, Tallant DR, Martin SW. *J. Non-Cryst. Solids* 1998 ; **223** : 21.

[16] Swenson J, Matic A, Brodin A, Börjesson L, Howells WS. *Phys. Rev. B* 1998 ; **58** : 11331.

[17] Le Saoût G, Vaills Y, Luspin Y. *Solid State Comm.* 2002 ; **123** : 49.

[18] Lines ME. *J. Non-Cryst. Solids* 1987 ; **89** : 143.

[19] Lines ME, Miller AE, Nassau K, Lyons KB. *J. Non-Cryst. Solids* 1987 ; **89** : 163.

[20] Matic A, Börjesson L. *Phil. Mag. B* 1998; **77**: 357.

[21] Bobovich YS. *Opt. Spectrosc*. 1962; **13**: 274.

[22] Efimov E. *J. Non-Cryst. Solids* 1997 ; **209** : 209.

[23] Efimov E. *J. Non-Cryst. Solids* 1998 ; **232-234** : 99.

[24] Mayerhöfer TG, Dunken HH, Keding R, Rüssel C. *J. Non-Cryst. Solids* 2004 ; **333** : 172.

	$(ZnO)_{0.6}(P_2O_5)_{0.4}$ x=0				$(PbO)_{0.}(ZnO)_{0.3}(P_2O_5)_{0.4}$ x=0.3				$(PbO)_{0.6}(P_2O_5)_{0.4}$ x=0.6				*Assignment*
j	ω_{jTO}	Γ_{jTO}	ω_{jLO}	Γ_{jLO}	ω_{jTO}	Γ_{jTO}	ω_{jLO}	Γ_{jLO}	ω_{jTO}	Γ_{jTO}	ω_{jLO}	Γ_{jLO}	
8	922	52	945	88	907	55	928	85	889	55	909	84	ν_{as}(P-O-P)
9	1003	54	1006	60	976	42	977	47	957	29	958	31	$\nu_s(PO_3)^{2-}$
10	1080	110	1105	112	1073	89	1091	128	1052	81	1060	147	$\nu_{as}(PO_3)^{2-}$
11	1160	150	1165	130	1160	132	1166	81	1142	110	1151	50	$\nu_{as}(PO_3)^{2-}$
12	1230	148	1304	115	1210	138	1270	96	1202	135	1255	77	$\nu_{as}(PO_2)^-$

Table 1: Fit parameters used to describe the dielectric function in the 900-1500 cm^{-1} range for $(PbO)_x(ZnO)_{(0.6-x)}(P_2O_5)_{0.4}$ glasses.

$(PbO)_{0.6}(P_2O_5)_{0.4}$ (x=0.6) *Band frequency (cm^{-1})*		*Assignment*
R	*IR (TO-LO)*	
686 727 *774*	699-705 *755-758*	ν_s(P-O-P)
887	889-909	ν_{as}(P-O-P)
926		$\nu_s(PO_4)^{3-}$
966	*957-958*	$\nu_s(PO_3)^{2-}$
1017		$\nu_s(P_2O_7)^{4-}$
1049	1051-1060	$\nu_{as}(PO_3)^{2-}$
1088		$\nu_s(PO_2)^-$, $(P_2O_7)^{4-}$
	1142-1151	$\nu_{as}(PO_3)^{2-}$
1133		$\nu_s(PO_2)^-$
1198	1202-1255	$\nu_{as}(PO_2)^-$

Table 2: Raman and IR band assignments in the 600-1500 cm^{-1} range for $(PbO)_{0.6}(P_2O_5)_{0.4}$ glasses (weak intensities are in italic).[12]

Figure Captions

Figure 1: IR reflection spectra of $(PbO)_x(ZnO)_{(0.6-x)}(P_2O_5)_{0.4}$ glasses.

Figure 2: Imaginary parts of the dielectric (—) and the inverse dielectric (---) functions (a) and reduced Raman spectra (b) of the $(PbO)_x(ZnO)_{(0.6-x)}(P_2O_5)_{0.4}$ glasses.

Figure 3: Lead content dependence of the $\nu_{as}(PO_2)^-$, $\nu_{as}(PO_3)^{2-}$, $\nu_{as}(POP)$ deduced from IR spectra (TO mode are in plain symbol and LO in open symbol) (a) and $\nu_s(PO_2)^-$, $\nu_s(POP)$ deduced from Raman spectra (b) in the $(PbO)_x(ZnO)_{(0.6-x)}(P_2O_5)_{0.4}$ glasses.

Figure 4: Lead content dependence of the Γ_j (a) and $\Delta\varepsilon_j$ (b) deduced from IR simulation spectra in the $(PbO)_x(ZnO)_{(0.6-x)}(P_2O_5)_{0.4}$ glasses.

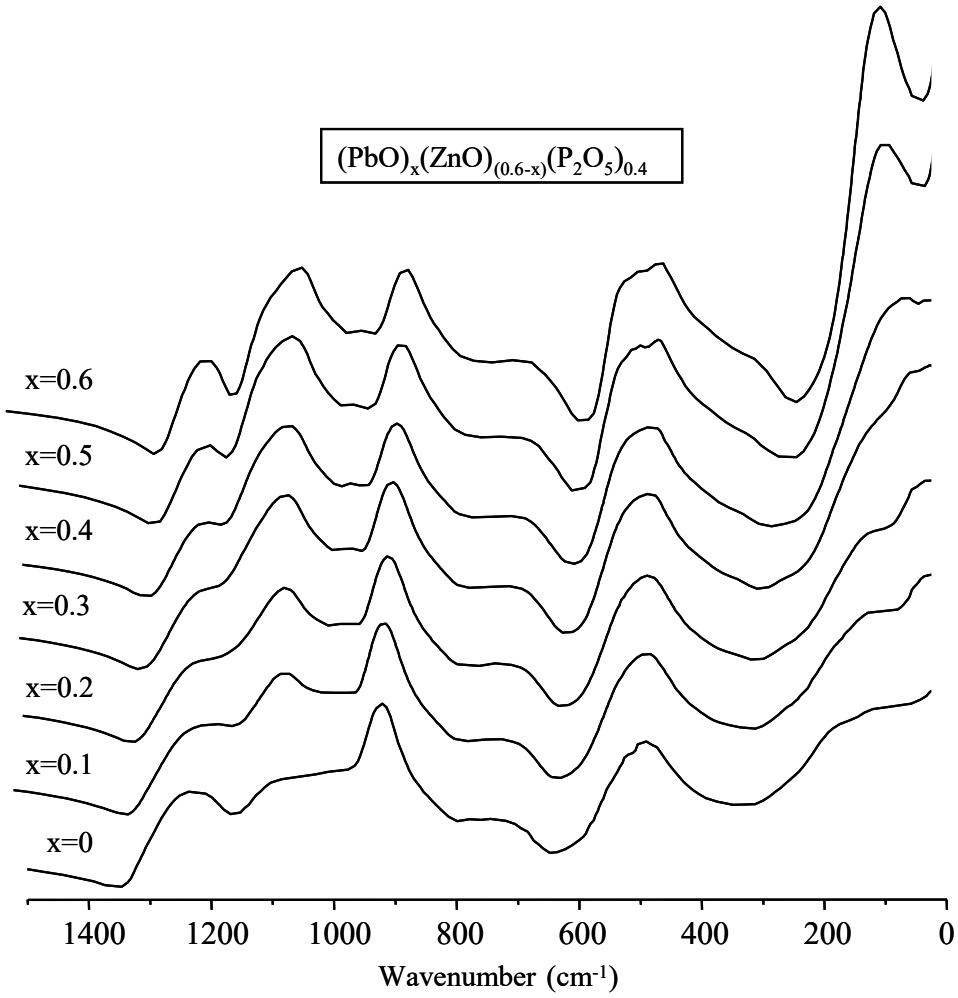

Figure 1: IR reflection spectra of $(PbO)_x(ZnO)_{(0.6-x)}(P_2O_5)_{0.4}$ glasses.

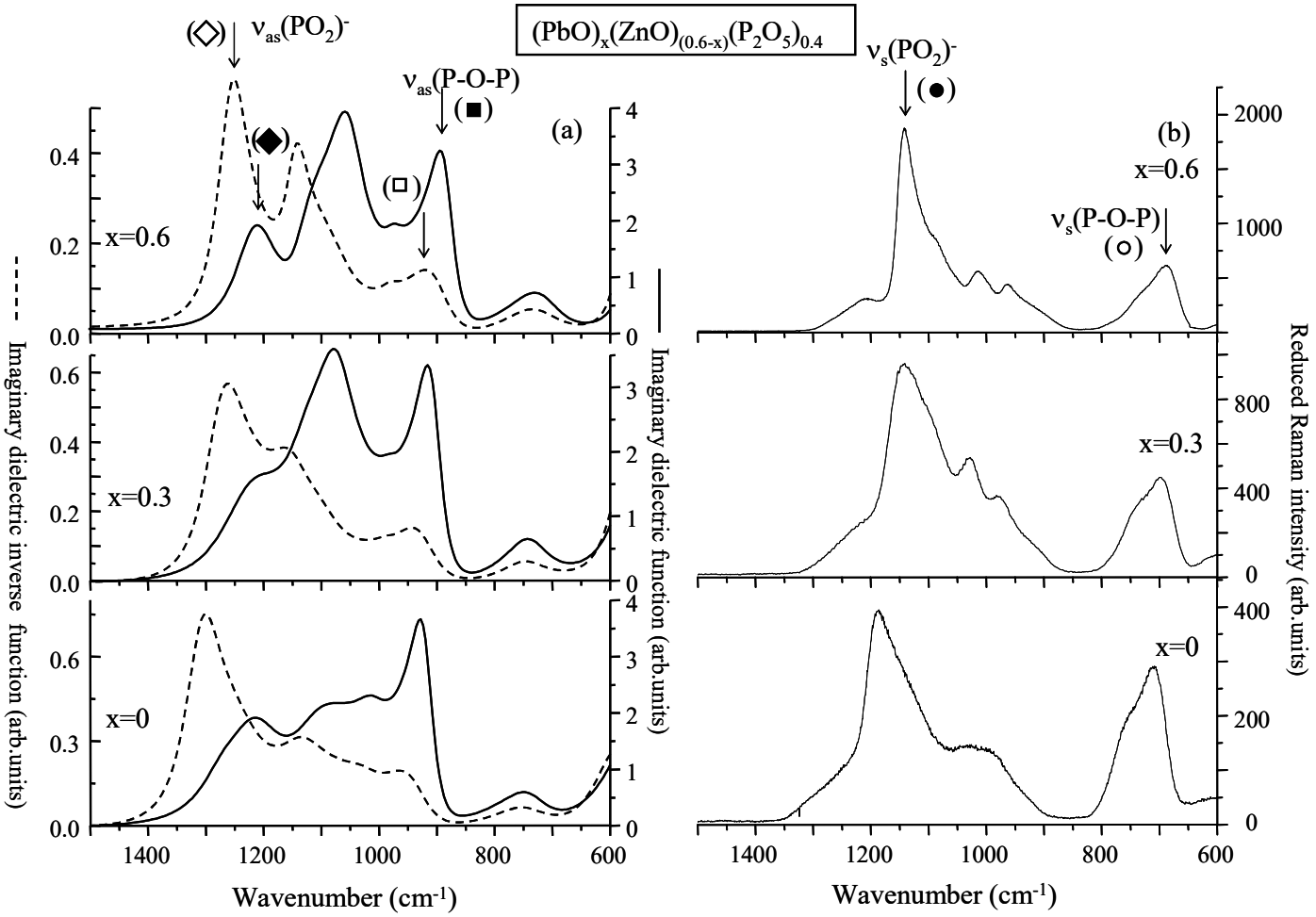

Figure 2: Imaginary parts of the dielectric (—) and the inverse dielectric (---) functions (a) and reduced Raman spectra (b) of the $(PbO)_x(ZnO)_{(0.6-x)}(P_2O_5)_{0.4}$ glasses.

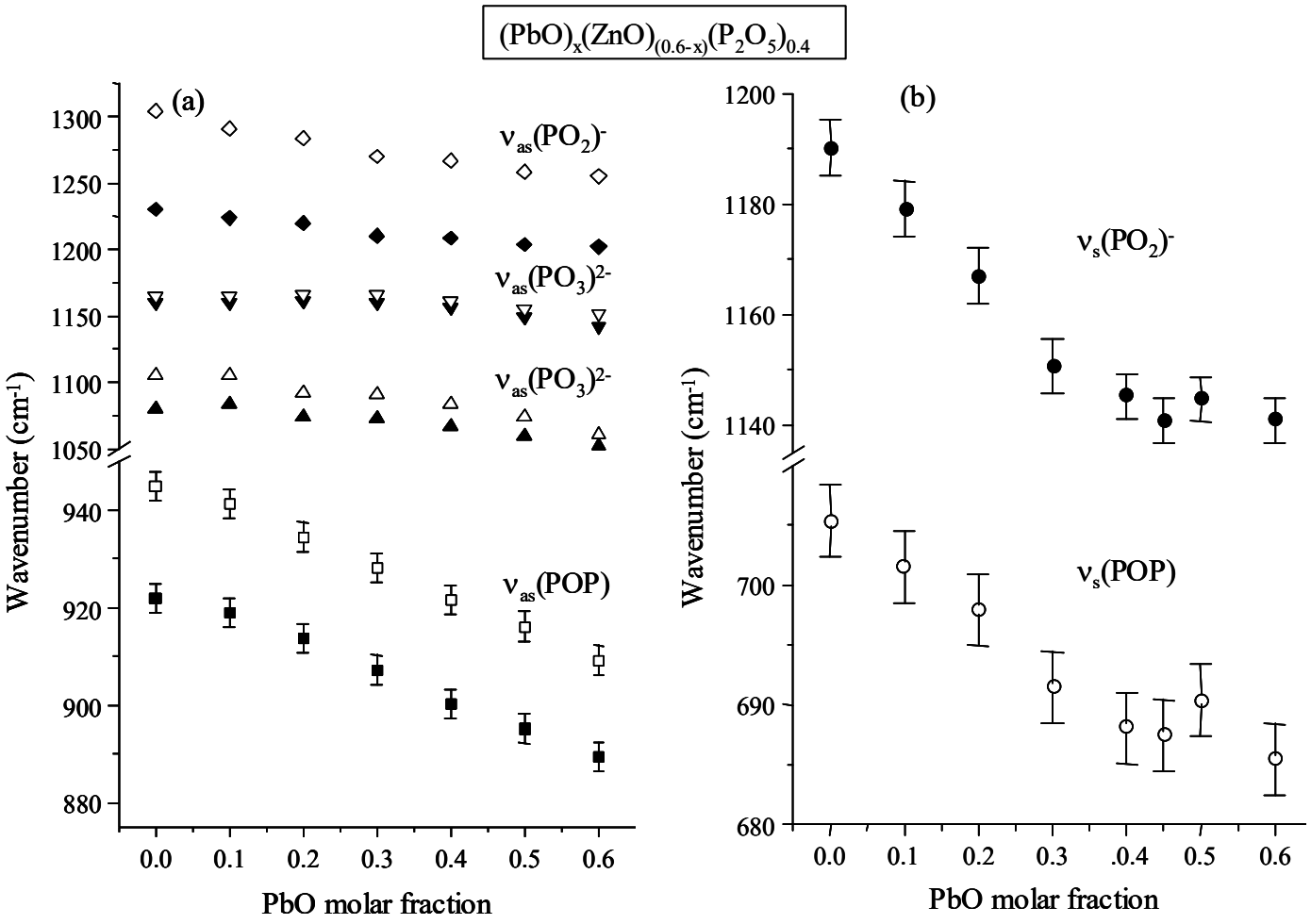

Figure 3: Lead content dependence of the $\nu_{as}(PO_2)^-$, $\nu_{as}(PO_3)^{2-}$, $\nu_{as}(POP)$ deduced from IR spectra (TO mode are in plain symbol and LO in open symbol) (a) and $\nu_s(PO_2)^-$, $\nu_s(POP)$ deduced from Raman spectra (b) in the $(PbO)_x(ZnO)_{(0.6-x)}(P_2O_5)_{0.4}$ glasses.

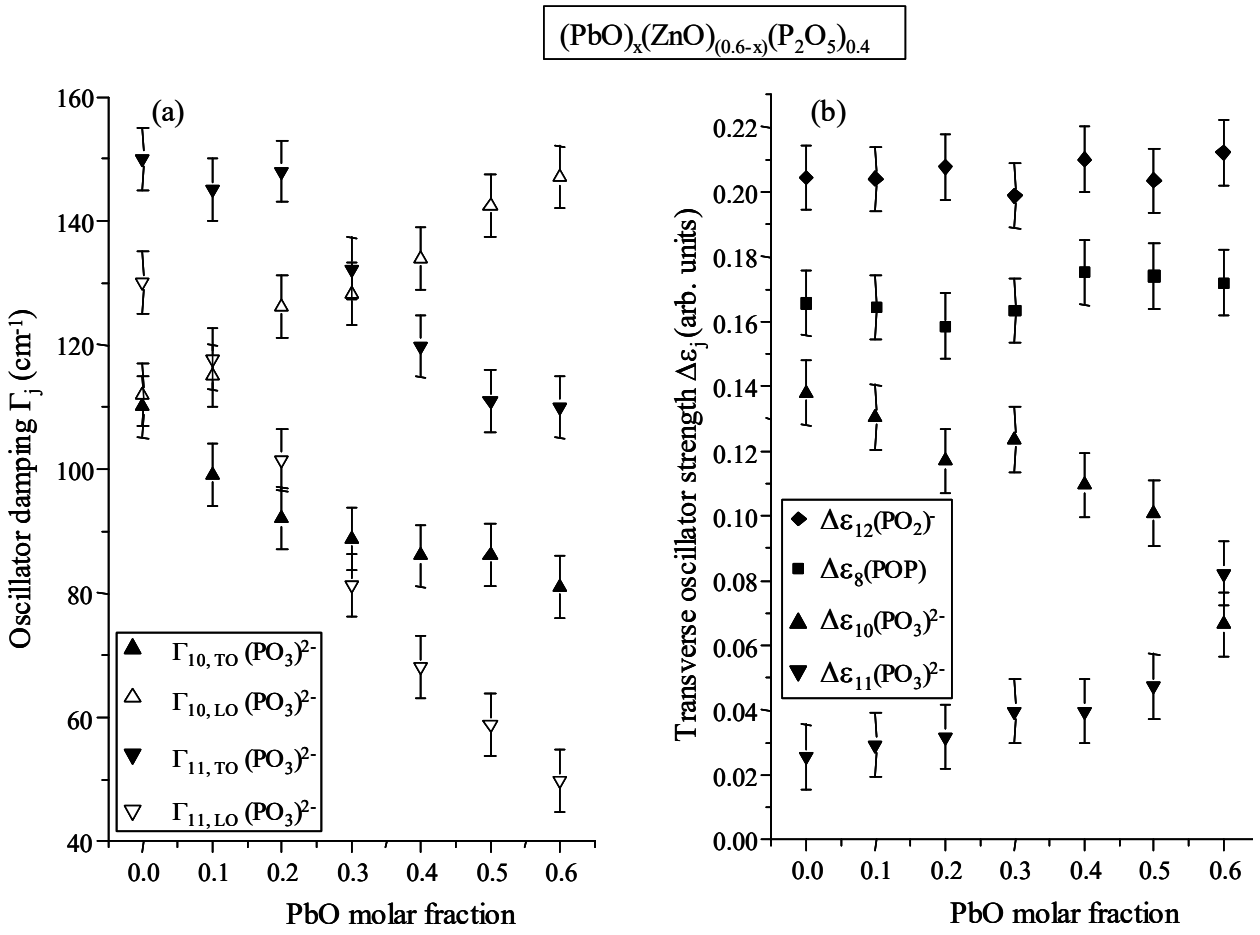

Figure 4: Lead content dependence of the Γ_j (a) and $\Delta\varepsilon_j$ (b) deduced from IR simulation spectra in the $(PbO)_x(ZnO)_{(0.6-x)}(P_2O_5)_{0.4}$ glasses.

Table of contents entry

Paper title and Authors

Raman and Infrared Structural Investigation of $(PbO)_x(ZnO)_{(0,6-x)}(P_2O_5)_{0,4}$ glasses

G. Le Saoût, P. Simon*, F. Fayon, A. Blin, Y. Vaills

Text:

Structure of $(PbO)_x(ZnO)_{(0,6-x)}(P_2O_5)_{0,4}$ glasses: The structure of $(PbO)_x(ZnO)_{(0,6-x)}(P_2O_5)_{0,4}$ glasses has been investigated using Raman scattering and infrared spectroscopy. The intensity variation in the high frequency part of the Raman and IR spectra are attributed to an effect of the Zn/Pb substitution on the vibrational mode of the phosphate chain rather than a variation of the chain length with PbO content.

Figure